

# Multi-Mode Wave Orbit for Multigigabit Transmission via Rotary Transmitter with a Free Rotation Center

**Abstract**—The development of semiconductor devices in the millimeter-wave and sub-terahertz range and the associated development of broadband wireless standards offer a promising alternative to the state-of-the-art design of rotary transmitters with free rotation centers based on transmission technologies in the baseband. A novel approach will be used to find a way to use upcoming transmission standards to build a multi-gigabit rotary transmitter. Channel models of a so-called multi-mode wave orbit were developed to determine and optimize the key characteristics of the novel channel. A test setup has been used to measure the channel and compare it to the model. It could be shown that with the help of several optimizations, a channel can be created that provides a stable channel capacity of over 10 Gbps at a bandwidth of 1.76 GHz for diameters of 1.1 m at over 100 rpm. Due to the simple construction and the possibility to use off-the-shelf components, this approach becomes interesting for a variety of rotary transmitter applications.

**Keywords**—Millimeter waves, rotary transmitter, slip ring, rotary joint, 802.11ad, 802.11ay, multi path channel model, delay spread, channel capacity, channel impulse response

## I. INTRODUCTION

Many applications require the transmission of data at high rates via rotating parts. A particular challenge arises with a rotary transmitter that has a free rotation center. In such a case, the coupling cannot take place in the center of rotation, therefore the data must be routed around the free rotation center and decoupled at any point of the ring. This is especially relevant when high data rates with short symbol times and large free inner radii are required. If the circumference is not electrically short, the transmission line lengths are no longer negligible. To ensure a transmission channel without multipath propagation and without phase discontinuities, the topology shown in Figure 1 is typically used. [1]

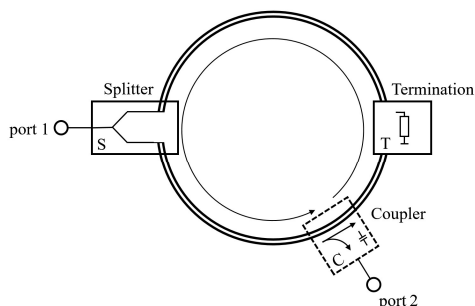


Fig. 1. State of the art topology of a multi-gigabit rotary transmitter with free rotation center (dashed line for rotating parts and solid line for fixed parts).

In practice, the maximum data rate is physically limited to about 10 Gbps. Only with the help of complex topologies consisting of short line segments and proprietary signal and packet processing at higher OSI levels, this physical limit can be counteracted. [1,2,3]

Edholm's law states a doubling of the data rate of communication standards approximately every 18 months [4]. [5] predicts that due to the rapid development of millimeter wave technology, wireless standards with 100Gbps will be available by 2025. Rotary transmitter applications can benefit from this development in that transmission technology available on the market can be deployed, dispensing with development of demanding custom-made solutions.

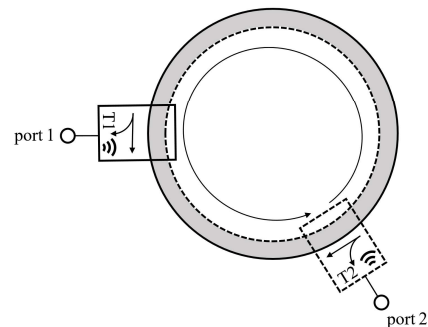


Fig. 2. Basic topology of a Multi-Mode Wave Orbit (dashed line for rotating parts and solid line for fixed parts).

We investigated a novel topology illustrated in Figure 2, in which standardized wireless technology with high throughput, according to IEEE standards 802.11ad [6] or 802.11ay, is applied. It consists of two metal cylinders which, when inserted into each other, form a circular cavity. Cutouts in the metal walls allow the signal to be fed in and out and the signal is reflected between the metal walls along the cavity. This structure is referred to in the following as Multi-Mode Wave Orbit (MMWO).

## II. CHANNEL MODEL

A channel model has been developed to estimate the channel characteristics and the influences of the system parameters. The model is purely deterministic, since it uses only the information from a geometric ray model, only, to determine the channel impulse response.

The latter is given by

$$h(t) = \sum_{k=1}^N a_k(t) \cdot e^{-j2\pi f_c \tau_k(t)} \cdot \delta(t - \tau_k(t)) \quad (1)$$

according to the conventional multipath fading channel model for  $N$  paths, where the gain  $a_k(t)$  and the delay  $\tau_k(t)$  of path  $k$  are time-dependent due to the rotary motion. This also allows effects such as small scale fading to be taken into account. This work will initially be limited to a quasi-static analysis of the channel.

Two models based on (1) were developed, the linear MMWO model and the rotary MMWO model. The linear MMWO model was created because it is easier to validate on a test stand, while following the same modeling principle as the rotary model. The main difference of the linear model vs. the rotary model is that all paths are propagable and there are no multiple orbits.

#### A. Simplified Linear Model of the MMWO

The linear model depicts two parallel plates, with constant distance  $s$ , with two transceivers directed towards each other, displaced by the offset  $d_{shift}$ .

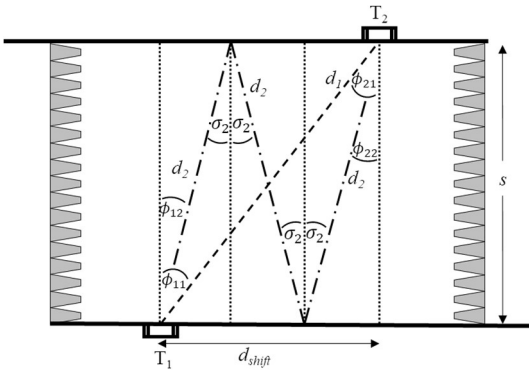


Fig. 3. Side view of a linear MMWO with two example paths for  $k=1$  and  $k=2$ .

As illustrated in Fig. 3, each propagation path  $k$  between transceiver T1 to T2 undergoes the number of subpaths

$$\xi = (2 * k - 1). \quad (2)$$

Considering a further shift  $d_{ax}$  orthogonal to the viewing plane of Fig. 3, the path lengths become

$$d'_k = \xi d_k^* = \xi \sqrt{\frac{d_{ax}^2}{\xi^2} + d_k^2} = \xi \sqrt{\frac{d_{ax}^2}{\xi^2} + \left(s^2 + \frac{d_{shift}^2}{\xi^2}\right)} \quad (3)$$

for each path  $k$ . The path delay is  $\tau_k = \frac{d'_k}{c}$ , where  $c$  is the propagation velocity of the free space.

The elevation angle for both transceivers is

$$\Theta_{1k} = -\Theta_{2k} = \arctan\left(\frac{d_{shift}}{s}\right) \quad (4)$$

and their azimuth angle is given by

$$\phi_{1k} = -\phi_{2k} = \arctan\left(\frac{d'_k}{d_{ax}}\right), \quad (5)$$

assuming that the transceivers face each other at  $d_{shift} = 0$ .

The path loss then becomes

$$\begin{aligned} L_{k\ dB} &= -a_{k\ dB} \\ &= 20 \log_{10} d'_k + 20 \log_{10} f_c + 20 \log_{10} \left(\frac{4\pi}{c}\right) \\ &\quad - G_{dB}(\Theta_{ant1k}, \phi_{ant1k}) \\ &\quad - G_{dB}(\Theta_{ant2k}, \phi_{ant2k}) + (\xi - 1)R_{dB} \\ &\quad + L_{antk\ dB} + d'_k L_{oxy\ dB/m}, \end{aligned} \quad (6)$$

with the gain of each transceiver  $G_{dB}$ , the reflection attenuation  $R_{dB}$ , the attenuation caused for paths  $k$  with small angle  $\Theta$  by reflection on the same antenna surface  $L_{antk\ dB}$  and the additional attenuation by oxygen absorption at 60 GHz of about 0.01 dB/m.

#### B. Complete Rotary Model of the MMWO

The actual MMWO setup is represented by the rotary MMWO model illustrated in Fig. 4 with one example path for each sense of rotation  $\zeta$ , which is 1 for clockwise and 2 for ccw. rotation.

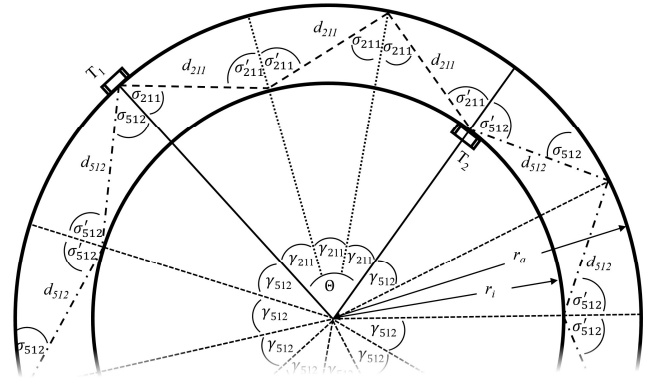


Fig. 4. Side view of a rotary MMWO with two example paths for  $k=2, v=1, \zeta=1$  and  $k=5, v=1, \zeta=2$ .

In comparison to (3), multiple path orbits  $v$  must be considered, resulting in path lengths

$$d'_{kv\zeta} = \xi d_{kv\zeta}^*, \quad (7)$$

which have three different indexes to distinguish the paths.

For the rotary MMWO model, the number of subpaths  $\xi$  can be determined by (2). The length of a single path segment between two reflections is given by

$$d_{kv\zeta}^* = \sqrt{\frac{d_{ax}^2}{\xi^2} + d_{kv\zeta}^2} = \sqrt{\frac{d_{ax}^2}{\xi^2} + \left((r_i \sin \gamma_{kv\zeta})^2 + (r_a - r_i \cos \gamma_{kv\zeta})^2\right)}, \quad (8)$$

where  $r_a$  and  $r_i$  are the outer and inner radius, respectively.

Each path causes the delay  $\tau_{kv\zeta} = \frac{d_{kv\zeta}^*}{c}$ . The angle of inclination of each path at T1 is

$$\sigma_{kv\zeta} = \arctan\left(\frac{r_i \sin \gamma_{kv\zeta}}{r_a - r_i \cos \gamma_{kv\zeta}}\right), \quad (9)$$

with the partial rotation angle given by

$$\gamma_{kv\zeta} = \frac{(2\pi - \Theta)(\zeta - 1) - (\zeta - 2)\Theta + 2\pi(v - 1)}{\xi} \quad (10)$$

in consideration of multiple path orbits  $v$ , the rotation angle  $\Theta$  and the sense of rotation  $\zeta$ . Equation (9) and (10) can be used to determine the angle of inclination at  $T_2$ :

$$\sigma'_{kv\zeta} = \sigma_{kv\zeta} + \gamma_{kv\zeta}. \quad (11)$$

In comparison to (4) and (5), the azimuth angle for both transceivers becomes

$$\phi_{1kv\zeta} = -\phi_{2kv\zeta} = \arctan\left(\frac{d'_{k\zeta v}}{d_{ax}}\right) \quad (12)$$

and the elevation angle in both propagation directions  $\Theta_{1kv1} = \sigma_{kv\zeta}$  and  $\Theta_{1kv2} = -\sigma_{kv\zeta}$  for transceiver T1 is different from the elevation angle  $\Theta_{2kv1} = -\sigma'_{kv\zeta}$  and  $\Theta_{2kv2} = \sigma'_{kv}$  for transceiver T2.

In addition to the general attenuation of (6), the attenuation of the complete rotary model of the MMWO  $L_{kv\zeta dB}$  must be extended by a multi orbit attenuation  $L_{moa dB}$  for each orbit that occurs when a path passes its own transmitting antenna. Since not all paths are propagable, it must be noted that (7-12) is only valid for  $v \in \mathbb{N}$ ,  $\zeta \in \{1,2\}$  and  $k \in \mathbb{N}: k > \frac{\Theta + 2\pi(v-1)}{2\arccos(\frac{r_i}{r_a})} + \frac{1}{2}$ .

### III. CHANNEL OPTIMIZATION

The channel model presented above is well suited for channel optimization due to its fast computation time. In this chapter, optimization of the rotary MMWO model is performed. Unless otherwise mentioned, the parameters from Table I were used for the optimization steps. All parameters concerning the transceivers are based on [6] and the test hardware used for the validation of the channel model. Special attention was paid during optimization to reducing the delay spread. This property turned out to be the bottleneck of the MMWO and can be improved by the combination of several strategies in such a way that transmission with conventional 802.11ad radio modules becomes possible.

TABLE I. BASIC CHANNEL PARAMETERS

Parameter	Value	Unit
Outer radius	$r_a$	0.574 m
Inner radius	$r_i$	0.550 m
Maximum number of paths $k$	$N$	400
Maximum number of orbits $v$	$\Upsilon$	4
Rotation angle	$\Theta$	180 °
Axial displacement	$d_{ax}$	0.025 m
Conductivity (aluminum)	—	36.9 MS/m
Multi orbit attenuation	$L_{moa dB}$	0 dB
SC chip rate [802.11ad]	$f_s$	1.760 GHz
Carrier frequency	$f_c$	60 GHz
Transmission power	$P_{TX}$	1 dBm

In the case of a rotary transmitter with a rotation speed of 100rpm, a radius of 55cm and 60GHz radio modules, the coherence time is 1.15ms. According to [6], the maximum transmission time of a packet  $\max_{TX\_time}$  is equal to 2ms. [7] measured the packet length of an 802.11ad radio module and observed that even at high throughput with maximum data aggregation, the packet length was never greater than 25  $\mu$ s. Based on the assumption that dynamic effects of the channel do not affect the transmission behavior, in the following, the channel is exclusively examined statically.

#### A. Plate Spacing

The first optimization strategy is to reduce the plate spacing. This significantly reduces  $\tau_{rms}$ . Fig.5 shows the change of  $\tau_{rms}$  when the plate spacing is changed between 0.01 m and 0.1 m at a fixed inner radius  $r_i$ . In case of air as dielectric medium, the plate spacing should be  $\gg \frac{\lambda}{2}$  to be different from a typical slab waveguide.

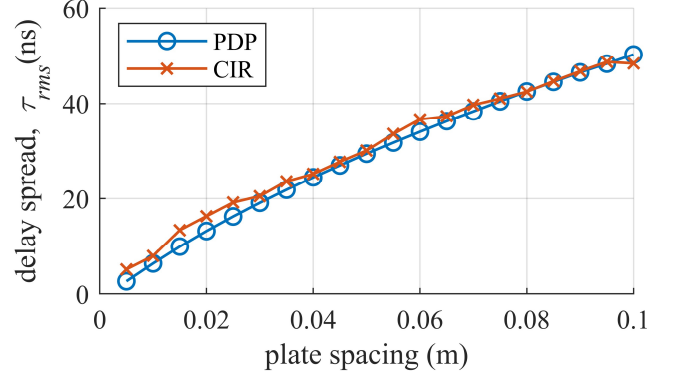


Fig. 5. Influence of the plate spacing on the delay spread for a MMWO with  $r_i=0.55$  m, quasi-omnidirectional beam pattern.

Furthermore, any path in direction of the main beam should not be reflected back on the same antenna itself. The test hardware employed has a maximum beam angle of 45° and a 38mm wide antenna array. Assuming a slightly shallower angle of about 38°, the minimum plate spacing becomes 24mm. This plate spacing thus allows for readjustment of the beam angle in both directions.

#### B. Reflection coefficient

Assuming that the reflection loss  $R_{dB}$  at each reflection is determined by the Hagen-Rubens relation [8] for the carrier frequency  $f_c$ , the relationship between DC conductance and channel capacitance shown in Fig. 6 can be found. In order to calculate the channel capacity, not only the signal to thermal noise ratio (STNR), but also the signal to quantization noise ratio (SQNR) and the signal to interference ratio (SIR) have been applied. [6] specifies a noise figure of 10 dB and an insertion loss of 5 dB for calculating the STNR. The effective number of bits (ENOB) is assumed to be 6, which limits the maximum channel capacity to about 21 Gbps. To calculate the SIR, a window of the width of the guard interval (GI) in the CIR is searched for, in which the power sum is maximum.

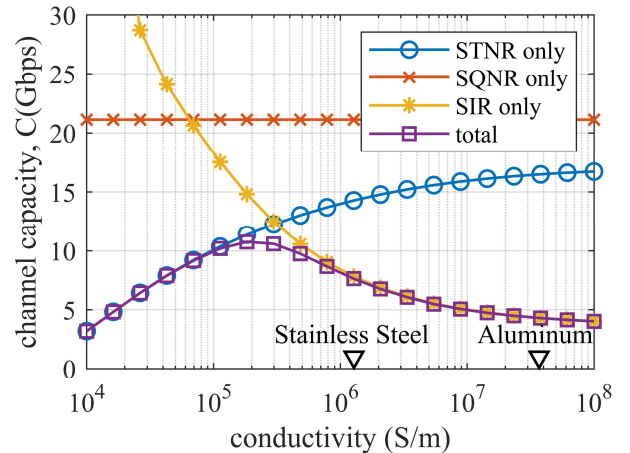


Fig. 6. Trade-off between attenuation and delay spread due to the conductivity of the reflective rings for a quasi-omnidirectional beam pattern.

At low conductance values, the STNR is dominant, whereas at high conductance values, the SIR defines the channel capacitance. In this configuration, the optimum is about  $2 \cdot 10^5 \frac{S}{m}$ . This corresponds to a conductivity of about one hundredth of aluminum. Since this reflection factor can be achieved by certain coatings or surface treatments only, this method is initially dispensed with for further optimization steps, and aluminum is used as a reflection material, instead.

### C. Radiation pattern

Instead of a quasi-omnidirectional radiation pattern, a directional radiation pattern can be used to restrict the transmit power to a few paths. The channel impulse response plotted in Fig. 7 shows that the peaks of each orbit can be separated easily if the directional beam pattern is used.

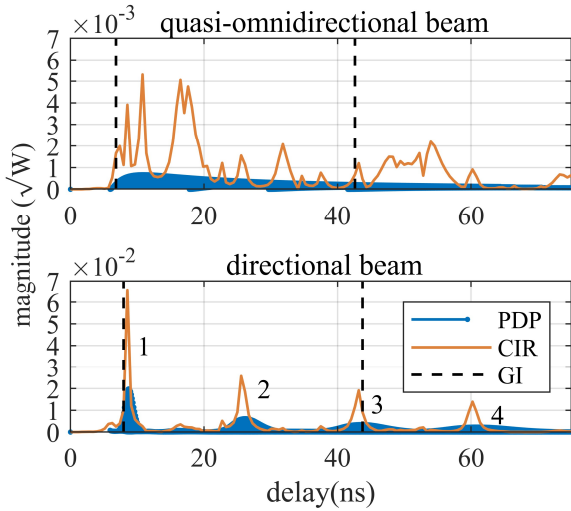


Fig. 7. Impact of a directional beam pattern on the channel impulse response.

The first peak marked with “1” is caused by paths with  $v = 1$ , the peak marked with “2” is caused by paths that have undergone a complete orbit with  $v = 2$ , and so on. In this model, data of beam pattern measurements of a beam with an azimuth angle of  $42^\circ$  and a half power beam width of approximately  $5^\circ$  are used.

### D. Multi-Orbit Attenuation

Since propagation predominantly occurs over one of the two circle segments when using a radiation pattern in one direction, the channel capacity limit is no longer at  $180^\circ$  but close to  $360^\circ$ . For the channel impulse response in Figure 8, an angle of  $300^\circ$  is chosen for better illustration. It can be seen that the small peak 1b appears next to the main peak 1a. This is due to the propagation over the second segment of the circle and only becomes apparent for angles close to  $360^\circ$ . That is because then the paths, despite the low gain of the side lobes of the radiation pattern, are so short that their attenuation is small.

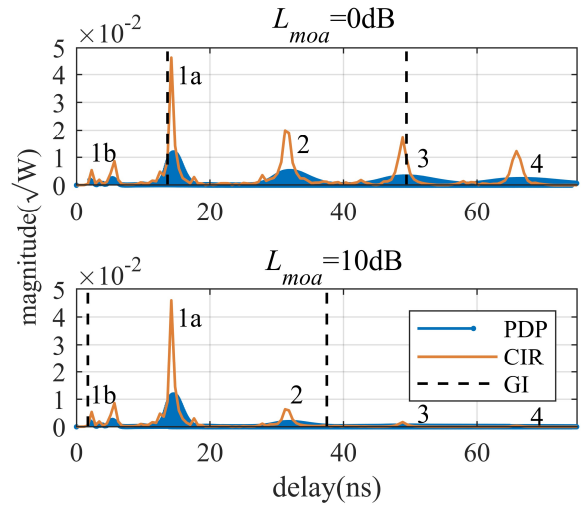


Fig. 8. Delay Spread reduction due to multi orbit attenuation.

In case of 802.11ad [6], the length of the GI is  $64 \cdot T_s = 36.4$  ns. A GI of 64 taps is not long enough to cover the peaks of multiple orbits and the peak 1b at the same time. To increase the signal to interference ratio it is important to reduce the power of the paths with multiple orbits. This can be achieved, for example, by applying absorber material in the area around the antenna structures. If paths have to pass this reflection point during the orbiting, an attenuation is caused. In case of an attenuation of  $L_{moa_{dB}} = 10$  dB, the SIR increases from 8.3 dB to 26.3 dB.

### E. Axial Displacement

By offsetting the transceivers in the axial direction, the transceivers are prevented from being exactly opposite to each other at a rotation angle of  $0^\circ$ . This reduces the receive power at low rotation angles and thus reduces the fluctuation of the receive power over one rotation. The demands on the control speed of the AGC of the receiver are thus reduced. Fig. 9 shows the receive power between an angle of  $0^\circ$  and  $150^\circ$ , without axial offset and with an axial offset  $d_{ax}$  of 25 mm, both with  $L_{moa_{dB}} = 10$  dB. The fluctuation of the receive power in this rotation range can be reduced from 20.5 dB to 10.6 dB by this measure.

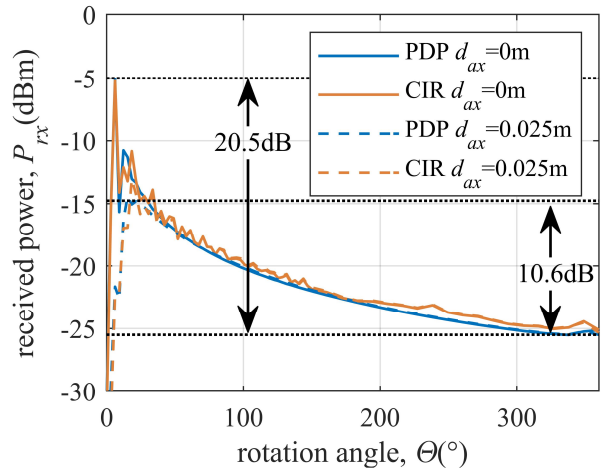


Fig. 9. Improvement of the fluctuation of the receive power by axial displacement.

#### IV. TEST SETUP

The simplified linear MMWO model should be validated using this test setup.

##### A. Hardware

The 60GHz WiGig modules from Fujikura shown in Fig. 10 were used as test hardware. They consist of two high gain phased array antennas with 4x16 elements, each, with a gain of 22 dBi for the TX and RX, a radio-frequency integrated circuit, a baseband processor, and a single board computer that provides a Gigabit Ethernet interface, as can be seen in Fig. 10b.

Using a secure shell protocol connection, the single board computer can be accessed to configure the modules to either start a throughput measurement between the radio modules using the iperf3 tool or to determine detailed status information, such as RX power, TX and RX modulation and coding schemes (MCS) or the channel impulse response determined by the Golay sequences of the control packet preamble.



Fig. 10. Fujikura 60GHz mmWave wireless communication module with customized mount. a) front view, b) side view.

##### B. Test Stand

The mechanical setup in Fig. 11 made it possible to set the plate spacing at a fixed distance and to change the shift distance  $d_{shift}$  manually or with the help of a motorized pulley in a continuous motion.

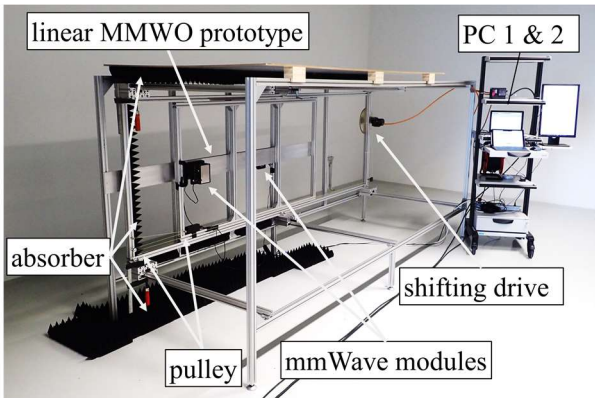


Fig. 11. Test stand for validating the simplified linear model of the MMWO.

In addition to the 12cm wide aluminum plate shown in Fig. 11, plate widths of 8, 10, 14, 16 and 100cm were also tested. The results did not show significant differences between the widths. For later validation, measurement results of the 100 cm wide plates were used, only.

#### V. MEASUREMENT RESULTS AND MODEL VALIDATION

The measurement results have been compared to the model, which was equally configured according to Table 1, such as a plate spacing of 24mm, a TX power of 1 dBm and an axial displacement  $d_{ax}$  of 25 mm.

##### A. Receive Power

With a resolution of the shift distance  $d_{shift}$  of about 3.3 mm, the power sum of the CIR and the PDP was calculated using the simplified linear MMWO model and plotted in Fig. 12 together with the receive power measured with the radio modules. For shift distances larger than 10 cm, there is a clear agreement between the trend of the measurements and the model.

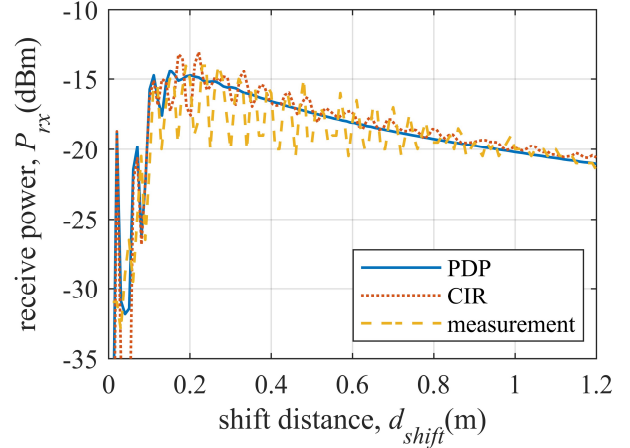


Fig. 12. Model comparison with measurement results regarding the received power.

The far field condition is fulfilled above a distance of about 0.6m. This also corresponds approximately to the shift distance, above which the fluctuations no longer occur and the model gets a closer agreement with the measurements. Within the reactive near field, the model is no longer applicable, as can be seen from Fig. 12 below distances of about 10 to 20 cm. This area needs to be investigated with a different approach.

##### B. Channel Impulse Response

The CIR was measured at a shift distance  $d_{shift}$  of 0.39 m.

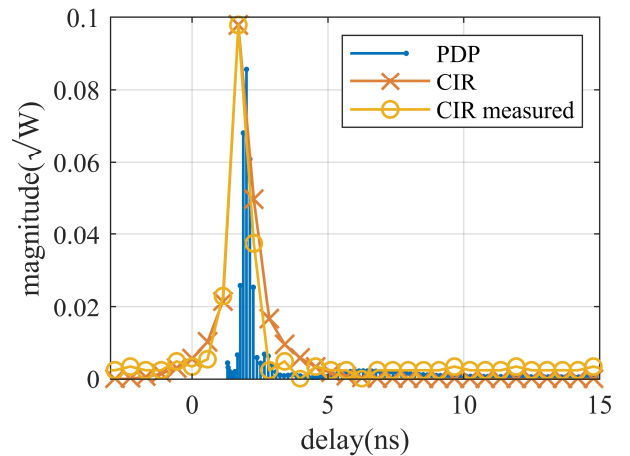


Fig. 13. Comparison of modeled and measured channel impulse response.

As can be seen in Fig. 13, the measured and modeled CIR show high agreement. It should be mentioned that the CIR is measured normalized and without absolute time. Therefore,

for better comparison, it was renormalized and shifted to the main value of the modeled CIR in Fig. 13.

### C. Throughput

Throughput measurements with iperf3 resulted in a net data rate of 3 Gbps over the entire shift from 0 to 1.2m. The automatically controlled MCS also remained at 12 and supported a gross data rate of 4.68 Gbps.

## VI. CHANNEL PERFORMANCE ESTIMATION

Using the complete rotary model of the MMWO with the optimized and validated configurations, estimates of channel capacity were made for common diameters of a rotary transmitter with free center of rotation and compared in Fig. 14.

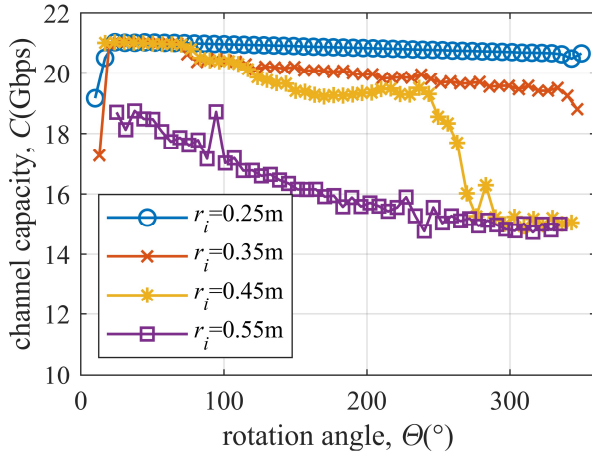


Fig. 14. Channel capacity estimation of a MMWO with 1.76 GHz Bandwidth.

Smaller diameters are limited almost exclusively by quantization noise for the entire rotation, whereas for a diameter of 1.1m, the data rate drops to about 15 Gbps at near 360°. At higher diameters, the data rate collapses almost completely since the GI can no longer capture all strong paths, as shown in Fig. 8. The data rate of 4.68 Gbps is therefore far below the channel capacity of the rotary transmitter, which suggests that higher order modulation could also be used if the standard allowed it. The 802.11ay standard comes with further features such as the possibility to bond up to four channels, to use 256 QAM modulation and to work with spatial streams, which would allow transmission in both propagation directions of the MMWO [9]. With these features, data rates of up to 74.8 Gbps could be possible. Transceivers using THz technology could bond much more channels to increase the channel capacity even further [10].

## VII. CONCLUSION

The idea of the novel Multi-Mode Wave Orbit (MMWO) has been presented. This allows to use widely available transmission technology according to present and future wireless communication standards to build rotary transmitters with a free rotation-center at data rates of several 10Gbps. A generic channel model of the MMWO has been presented, which allows for adaption of the MMWO to the properties of the wireless transmission system applied. The concept of the MMWO and the validity of the channel model could be verified with the aid of a simplified prototype.

## REFERENCES

- [1] H. Schilling, Datenübertragungskonzepte für ein Brust-CT, Friedrich-Alexander-Universität Erlangen-Nürnberg (FAU), 2014, urn:nbn:de:bvb:29-opus4-54843 .
- [2] G. Lohr, „Anordnung zur Hochfrequenzübertragung zwischen beweglichen Teilen“. Deutschland Patent DE000019543558A1, 22 November 95.
- [3] G. Lohr, „Anordnung zur kontaktlosen Drehübertragung hochfrequenter Signale“. Deutschland Patent DE10037747A1, 2 August 2000.
- [4] S. Cherry, "Edholm's law of bandwidth," in IEEE Spectrum, vol. 41, no. 7, pp. 58-60, July 2004, doi: 10.1109/MSPEC.2004.1309810.
- [5] H. Elayan, O. Amin, B. Shihada, R. M. Shubair and M. -S. Alouini, "Terahertz Band: The Last Piece of RF Spectrum Puzzle for Communication Systems," in IEEE Open Journal of the Communications Society, vol. 1, pp. 1-32, 2020, doi: 10.1109/OJCOMS.2019.2953633.
- [6] "IEEE Standard for Information technology--Telecommunications and information exchange systems--Local and metropolitan area networks--Specific requirements--Part 11: Wireless LAN Medium Access Control (MAC) and Physical Layer (PHY) Specifications Amendment 3: Enhancements for Very High Throughput in the 60 GHz Band," in IEEE Std 802.11ad-2012 (Amendment to IEEE Std 802.11-2012, as amended by IEEE Std 802.11ae-2012 and IEEE Std 802.11aa-2012) , vol., no., pp.1-628, 28 Dec. 2012, doi: 10.1109/IEEESTD.2012.6392842.
- [7] G. Bielsa, A. Loch, I. Tejado, T. Nitsche and J. Widmer, "60 GHz Networking: Mobility, Beamforming, and Frame Level Operation from Theory to Practice," in IEEE Transactions on Mobile Computing, vol. 18, no. 10, pp. 2217-2230, 1 Oct. 2019, doi: 10.1109/TMC.2018.2875095.
- [8] R. E. Hummel, Electronic Properties of Materials, Fourth Edition, University of Florida, Springer, 2010
- [9] Y. Ghasempour, C. R. C. M. da Silva, C. Cordeiro and E. W. Knightly, "IEEE 802.11ay: Next-Generation 60 GHz Communication for 100 Gb/s Wi-Fi," in IEEE Communications Magazine, vol. 55, no. 12, pp. 186-192, Dec. 2017, doi: 10.1109/MCOM.2017.1700393.
- [10] Gonzalez-Jimenez, J.L., Dehos, C., Cassiau, N. et al. Channel-bonding CMOS transceiver for 100 Gbps wireless point-to-point links. J Wireless Com Network 2020, 117 (2020). <https://doi.org/10.1186/s13638-020-01741-1>